

Vertical Land Motion from Present-Day Deglaciation in the Wider Arctic

Carsten Ankjær Ludwigsen¹, Shfaqat Abbas Khan¹, Ole Baltazar Andersen¹ and Ben Marzeion²

¹DTU Space, Technical University of Denmark

²Institute of Geography and MARUM – Center for Marine Environmental Sciences, University of Bremen, Germany

Key Points:

- Elastic VLM from present-day ice loss in the Arctic causes significant uplift of coastlines in North America and Northern Europe.
- A combined VLM-model that includes GIA and elastic VLM, yields good agreement with GNSS-stations in the wider Arctic.
- Residuals between GNSS and modeled VLM provides an approximation of extraordinary VLM caused by local circumstances.

Corresponding author: Carsten Ankjær Ludwigsen, caanlu@space.dtu.dk

Abstract

Vertical land motion (VLM) from past and ongoing glacial changes can amplify or mitigate ongoing relative sea level change. We present a high resolution VLM-model for the wider Arctic, that includes both present-day ice loading (PDIL) and glacial isostatic adjustment (GIA). The study shows that the non-linear elastic uplift from PDIL is significant ($0.5\text{--}1\text{ mm y}^{-1}$) in most of the wider Arctic and exceeds GIA at 15 of 54 Arctic GNSS-sites, including sites in non-glaciated areas of the North Sea region and the east coast of North America. Thereby the sea level change from PDIL (1.85 mm y^{-1}) is significantly mitigated from VLM caused by PDIL. The combined VLM-model was consistent with measured VLM at 85% of the GNSS-sites ($R=0.77$) and outperformed a GIA-only model ($R=0.64$). Deviations from GNSS-measured VLM can be attributed to local circumstances causing VLM.

Plain Language Summary

From 2003 to 2015, the Northern Hemisphere lost more than 6,000 gigatons of land ice, which added nearly 18 mm to the global mean sea level rise. Loss of land-based ice results in the vertical deformation of the Earth's surface. Ongoing rebounding or subsidence caused by the end of the last ice age is often assumed to govern vertical deformation. However, present-day ice loss from Greenland and Arctic glaciers also cause an immediate vertical deformation. By using an vertical deformation model, that includes both components, we can explain GPS-measured deformation occurring in the Arctic. Our results show that the present-day Arctic ice loss contribution to vertical deformation is approximately $0.5\text{ to }1\text{ mm y}^{-1}$ in the wider northern region. This exceeds deformation caused by the disappearance of the last ice ages at many coastal regions, including the North Sea region and the North American Atlantic coast. The Arctic present-day ice loss included in the VLM-model equals a global sea level rise of 1.5 mm y^{-1} , which means that 30-80% of the sea level rise caused by Arctic ice loss is mitigated by surface uplift caused by the same ice loss.

1 Introduction

The Arctic region is warming faster than any other region on Earth (Post et al., 2019). Deglaciation of Arctic land-based ice accounts for 70% of all barystatic sea level change (Abram et al., 2019) and has increased the sea level rise by 0.035 mm y^{-2} over the last three decades (Nerem et al., 2018). From 2003 to 2015 the Greenland Ice Sheet and adjoining glaciers produced 1 cm of sea level rise, while the contribution of other Arctic glaciers was 0.8 cm (Zemp et al., 2019).

Change in ice loading not only contributes to sea level change, but also alters Earth’s solid surface, which commonly is called Vertical Land Motion (VLM). Accurate quantification of VLM and its causes is key for understanding relative sea level (RSL) (Watson et al., 2015; Wöppelmann & Marcos, 2016), which is the sea level change measured by tide gauges (TG).

VLM can be modeled for a given ice loading by employing the sea level equation of Farrell and Clark (1976) or in its elastic adaptation by Clark and Lingle (1977). viscoelastic relaxation of Earth’s surface caused by past ice loading changes, also known as Glacial Isostatic Adjustment (GIA), has historically been the most important component of VLM (Farrell & Clark, 1976; Tushingham & Peltier, 1991; Milne & Mitrovica, 1998; Peltier et al., 2015) and is often assumed to be the key contributor to VLM in sea level studies from tide gauges (Church & White, 2011; Jevrejeva et al., 2014). This assumption is in particular inadequate in the Arctic region (Henry et al., 2012), where the change in present-day ice loading (PDIL) is extensive and the corresponding VLM equals GIA in order of magnitude.

Here we quantified the VLM resulting from changes in PDIL from 2003-2015 in the wider Arctic (the region above 50 deg latitude). After considering GIA, ocean loading, rotational feedback (RF) and non-secular geocenter motion, the total VLM uplift is predicted and compared to GNSS-measured VLM at 54 locations.

In recent years, data products from the Gravity Recovery And Climate Experiment (GRACE) satellite mission have been used to estimate PDIL and the corresponding VLM (Adhikari et al., 2016; Riva et al., 2017; Frederikse et al., 2019). While this is a reasonable estimate for regional and global VLM-patterns, the native resolution of GRACE is around 300-km half width at the equator (Tapley et al., 2004) which is insufficient for estimating VLM close to glaciers and ice sheets.

Here we combined a high-resolution (2x2 km) ice mass balance data in the Arctic to compute VLM from PDIL (VLM_{PDIL}), with a resolution that is suitable in both the near- and far-field in the Arctic region.

2 Data and Method

The solid-earth response of PDIL is assumed to be purely elastic and the viscoelastic response is considered to be negligible. This includes the ongoing solid-earth response from modern changes in ice loading prior to 2003, which is not considered in the applied GIA-models. In particular, the deglaciation after the Little Ice Age (LIA) that ended in the 19th century can create a GIA-like viscoelastic response that is not captured by GIA-models (Simon et al., 2018).

Contrary to studies using GRACE-measurements for ice loading, we used mass balance data from glaciers (Marzeion et al., 2012; Pfeffer et al., 2014; Zemp et al., 2019) that were transformed into an ice-elevation model (details in Supporting Information S1) with a 2x2 km spatial resolution by applying a mass balance distribution function and assuming a uniform density of 917 kg m^{-3} . Glaciers were combined with elevation changes from Greenland (updated version of the data from S. A. Khan et al. (2013), see section 2.1).

Separately, Antarctic yearly mass equivalent surface elevation changes for 2003-2015 from Schröder et al. (2019) were used to estimate the present-day Antarctic contribution to VLM in the Arctic.

The elastic VLM (VLM_{PDIL}) was computed with REAR (Regional Elastic Rebound calculator) (Melini et al., 2014, 2015). REAR calculates the elastic response to a disc load (Farrell, 1972) and assumes a solid, non-rotating and isotropic earth. Load Deformation Constants (LDC's) used for solving the Green's Functions were obtained from the REF6371 model by Kustowski et al. (2007) which is similar to the PREM-model (Dziewonski & Anderson, 1981), however the REF6371 model includes more realistic seismic properties of the crust (Kustowski et al., 2007). The LDC's from REAR are by default defined with respect to Earth's center of mass (CM-frame), which is consistent with the GIA-model of Caron et al. (2018). The ICE6G_D-model of Peltier et al. (2018) is referenced to the center of solid-earth (CE). The surface loading change included in GIA is however prehistoric and current viscoelastic mass transport induces a negligible CM-CE motion (King et al., 2012; Argus et al., 2014).

Rotational feedback (Milne & Mitrović, 1998) was added to the elastic VLM-model by using equation 1 and 2 from King and Watson (2014). Position changes of the pole (x_p, y_p) for ITRF2008 are available from IERS (Bizouard & Gambis, 2009). Since REAR is not solving the sea level equation (Farrell & Clark, 1976; Milne et al., 1999), it does not account for the effect of extra water mass added to the oceans because of PDIL, which results in a measurable deformation (van Dam et al., 2012; Santamaría-Gómez & Mémin, 2015). Non-tidal ocean loading (NOL) is predicted by estimating the elastic deformation of ocean bottom pressure (OBP, shown in Figure S2.2 in Supporting Information) grids from the latest version of Estimating the Circulation and Climate of the Ocean (ECCO) project (version 4, release 4) (Fukumori et al., 2019; Forget et al., 2015).

GNSS data are referenced to ITRF2008 (Altamimi et al., 2011), which has secular trends in CM, while non-secular trends of ITRF are in center of figure (CF) (Dong et al., 2003). Therefore, when studying ongoing mass changes, we need to make a ITRF to CM translation by considering non-linear geocenter motion (GCM). GCM is obtained from first-order Stokes coefficients from 2002-2019 provided by Sun et al. (2016) available from <https://grace.jpl.nasa.gov/data/get-data/geocenter/>, which are detrended in order to make the ITRF to CM translation. An VLM-model (eq. 2) is created that is comparable to adjusted GNSS-measured VLM (eq. 3):

$$VLM_{ela}^{CM} = VLM_{PDIL}^{CM} + VLM_{NOL}^{CM} + VLM_{rot} \quad (1)$$

$$VLM_{model}^{CM} = VLM_{GIA}^{CM} + VLM_{ela}^{CM} \quad (2)$$

$$VLM_{GNSS}^{CM} = VLM_{GNSS}^{ITRF} - GCM^{ITRF-CM} \quad (3)$$

Where VLM_{ela}^{CM} is the elastic VLM-model, VLM_{GIA}^{CM} represents VLM caused by GIA, VLM_{rot} indicates the deformation caused by rotational feedback and VLM_{NOL} is the contribution from NOL. VLM_{GNSS}^{CM} is GNSS-measured VLM after non-secular geocenter motion is removed. Average VLM-rates from 2003-2015 are shown in Figure 1, while VLM_{model}^{CM} is evaluated against VLM_{GNSS}^{CM} in section 3. The contribution of Antarctic ice loading (including Southern Hemisphere glaciers) is shown together with the contribution of VLM_{NOL}^{CM} and VLM_{rot} in Figure S2.1 in Supporting Information.

Caron2018 (Caron et al., 2018) is the default GIA-model throughout this study. Caron2018 used 128000 forward models of different 1D Earth rheologies and ice elevation histories to create a statistical distribution of the GIA signal representative of long term GNSS observations and relative sea level records from paleo RSL indicators. In some parts of the analysis, we include the ICE-6G_D GIA model of Peltier et al. (2018), since large discrepancies between the VLM_{model}^{CM} and VLM_{GNSS}^{CM} can be explained by the choice

of GIA-model. Recent study using an ensemble of simulations with 3D-earth rheologies (Li et al., 2020), seems to favor the results GIA-rates of Peltier et al. (2018).

Though we limited this study to the wider Arctic area, both the elastic VLM-components and GIA have a global impact. However, if we neglect the VLM caused by Antarctica, the VLM-signal from PDIL is relatively small ($< \pm 0.2 \text{ mm y}^{-1}$) outside the region of this study. The estimated uncertainty of the VLM_{model}^{CM} originates from the standard uncertainty of the ice model combined with a 10% uncertainty that represents the uncertainty from the REF6371 earth model (Wang et al., 2012).

While the ice model of Greenland is well constrained, mass balance errors of individual glaciers from the glacial model can be large (several times the glacial signal). We therefore divide the glacial model into $25 \times 25 \text{ km}$ tiles, which reduces the uncertainty significantly, but might also introduce unrealistic low uncertainty in areas with large glacial signals or where glaciers are poorly constrained. Glaciers are, however, still the largest source of regional uncertainty (see Supporting Information Figure S3.1.). The Caron2018 GIA-model has standard uncertainty estimates included in the product, while there is no uncertainty estimate associated with the ICE6G-model. Uncertainties of geocenter motion from Sun et al. (2016) contributes to the GNSS-uncertainty estimate. The spatial distribution of the uncertainty estimates are shown in Supporting Information Figure S3.1.

2.1 Ice Loading

The main component of VLM_{PDIL} is the ice loading model and consist of a combined water equivalent elevation model from Greenland and mass balance estimates from glaciers. Rate of elevation change is shown in Supporting Information Figure S1.1. While only Northern Hemisphere ice history is created with high resolution, changes of Antarctic and Southern Hemisphere ice loading is computed on a $0.5 \times 0.5^\circ$ grid and included in the computation of VLM_{PDIL}^{CM} . The low resolution does not have any impact on VLM in the Arctic. The total mass loss of the Southern Hemisphere is 140 Gt y^{-1} , equivalent of to 0.38 mm y^{-1} barystatic sea level rise.

2.1.1 Glaciers

A total of 62,000 individual glaciers from the Randolph Glacier Inventory (RGI 6.0) (Pfeffer et al., 2014; RGI Consortium, 2017) located in North America, Russia, Scandinavia (incl. Svalbard) and Iceland have been included in this study. Mass loss from included glaciers accounts for 95 % of the registered glacial mass loss of the Northern Hemisphere and constitutes 80% of the global glacial mass loss (Zemp et al., 2019).

Mass change estimates for each glacier were estimated using an updated version of a model reported in Marzeion et al. (2012). Direct mass balance observations (Zemp et al., 2019) were used to calibrate and validate the glacier model. The glacier model translates information about atmospheric conditions into glacier mass change, while considering various feedback mechanisms that occur between glacier mass balance and glacier geometry. Glacial mass balance was combined with a distribution function to calculate glacier-wide surface elevation change. This ensured that the lower parts of glaciers are thinning, while upper parts experience small elevation gains. This 'slope steepening' of glaciers is characteristic of glaciers of many regions (Nuth et al., 2010; Foresta et al., 2016; Ciraci et al., 2018) and is assumed to apply to all glaciers included in this study (see Supporting Information S1 for an enhanced description of glacial elevation change).

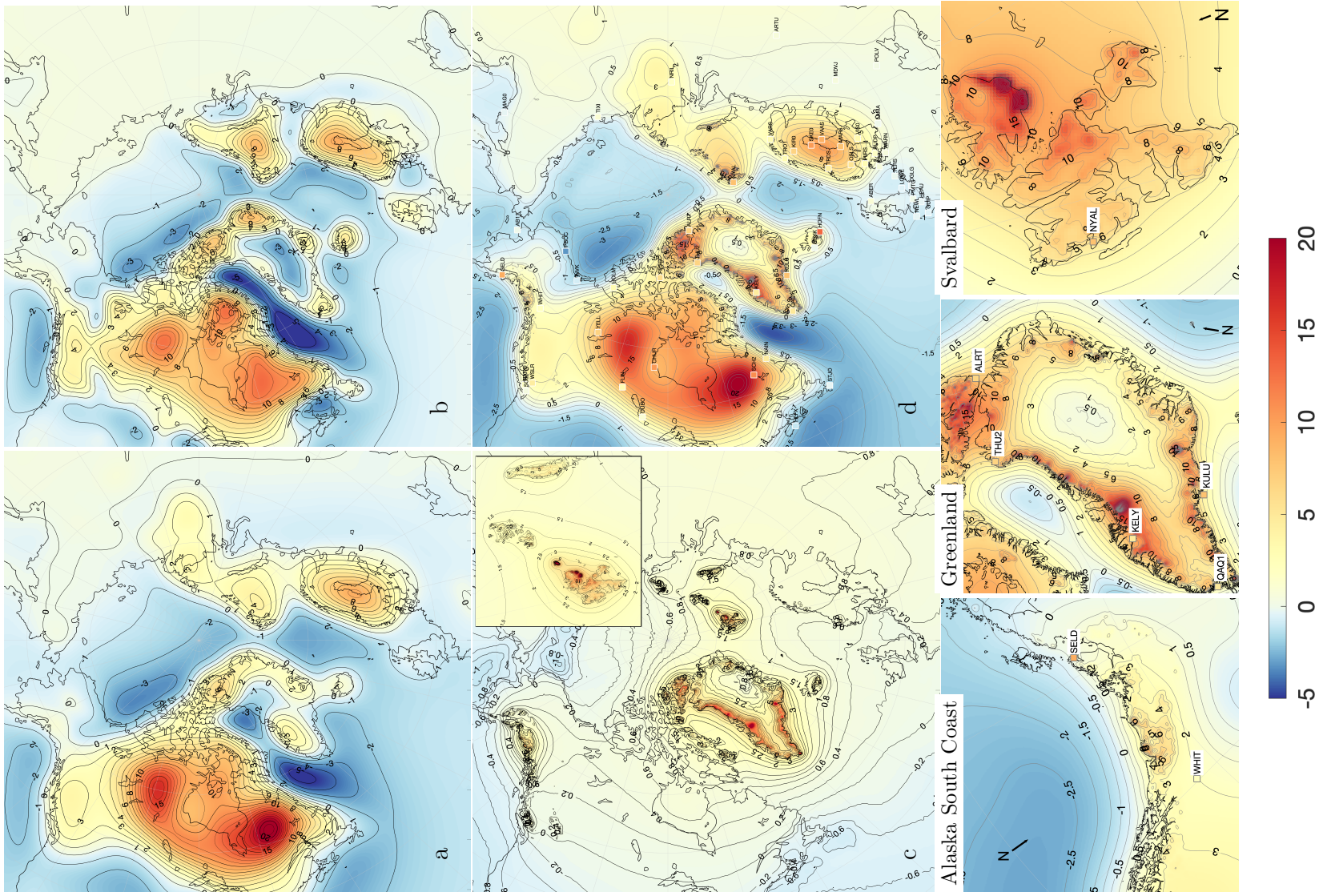


Figure 1. Average VLM-rates (mm y⁻¹) for 2003-2015 using the GIA-model of Caron2018(Caron et al., 2018) (a) and ICE6G_D (Peltier et al., 2018) (b). Modeled elastic rebound from contemporary land ice loss (including ocean loading and corrected for rotational feedback) (VLM_{CM}^{CM}) with enlargement of Svalbard is displayed in (c). The total VLM-model, VLM_{CM}^{CM}, (a + c), with the square coast of Svalbard is displayed in (d). Enlargements of the south coast of Alaska, Greenland and Svalbard of (d) is shown in the bottom three panels. Spatial distribution of uncertainty estimates of (a),(c) and (d) are shown in Supporting Information Figure S3.1.

2.1.2 Greenland

Glacial ice history was combined with elevation change of the Greenland Ice Sheet and adjoining glaciers. We estimated the rate of ice volume change from 2003-2015 by using altimeter surveys from NASA's ATM flights (Krabill, 2011) that took place between 2003 and 2015 supplemented with high-resolution Ice, Cloud and land Elevation Satellite (ICESat) data (Zwally et al., 2011) from 2003-2009 and CryoSat-2 data from 2011-2015 (Helm et al., 2014). Our procedure for deriving ice surface elevation changes has previously been described in detail by S. A. Khan et al. (2013) and is similar to the method used by, e.g. Ewert et al. (2012); Smith et al. (2009) and Kjeldsen et al. (2013). We used the observed ice elevation change rates to interpolate (using collocation) ice elevation changes onto the 2x2 km spatial grid.

2.2 GNSS data

Timeseries of vertical deformation and uncertainty estimates of 54 GNSS-sites from the sixth release of the consortium led by University of La Rochelle (ULR-6) (Santamaría-Gómez et al., 2017) were used. A detailed map and timeseries of all GNSS-sites are shown in Supporting Information Figure S4.1 and Figure S5.1. ULR-6 includes 125 GNSS-sites located within the area of interest, but only GNSS-sites with data for at least 120 of 156 months from 2003 to 2015 known not to be impacted by human activities were selected. One GNSS site was selected based on lowest observed standard deviation of timeseries when multiple GNSS sites were located within 100 km of each other. Nome (AT11), Esbjerg City (ESBC) and Magadan (MAG0) were exempted from the temporal selection criteria, because of their location which has a special interest for interpretation.

Annual averages and combined uncertainties were calculated for each GNSS-site from the vertical component and standard uncertainty included in ULR-6a. Hereafter, the linear trend was calculated for the years available between 2003 and 2015.

3 Evaluating the VLM model

From Figure 1 it is seen that the VLM-model is dominated by the pattern of the GIA-model, with rates above 20 mm y⁻¹ east of the Hudson Bay and another local maximum of over 15 mm y⁻¹ in north-west Canada. The elastic rebound is evident in most of the Arctic, particular in Greenland with large areas exceeding 10 mm y⁻¹, with maximum value at Jakobshavn Isbræ (69.1N, 49.5W) with an average modeled uplift of 40 mm y⁻¹. Large areas around Svalbard and Alaska have modeled elastic VLM-rates of more than 8 mm y⁻¹. The uncertainty is significantly larger in glaciated regions than in the far field (see Figure 3.1 in Supporting Information).

Most depression zones are found over the ocean, with the Beaufort Sea and Labrador Sea subsiding with 2 mm y⁻¹ and the Norwegian Sea with 1.5 mm y⁻¹. Subsiding coastal areas are found in North America, where Nova Scotia and most of the US east- and west coast subsides with more than 1 mm y⁻¹, while smaller subsidence (0.0 - 0.5 mm y⁻¹) is found in Northern Europe along the North Sea and Atlantic coastlines. From Figure 1 we see that most subsiding areas are caused by GIA.

Figure 2 shows that VLM_{model}^{CM} predicts VLM within the range of VLM_{GNSS}^{CM} at 46 of 54 GNSS locations considered. The mean absolute error (MAE) for the 54 GNSS-sites was 1.45 mm y⁻¹ (1.33 mm y⁻¹ for ICE6G_D), which was 0.53 mm y⁻¹ better than MAE from only VLM_{GIA} . For less than half (27) of the 54 GNSS-sites considered was the VLM-model with Caron2018 outperforming the ICE6G_D GIA model.

Barystatic sea level change for VLM_{PDIL} was 1.5 mm y⁻¹ (ice loss-mediated global average sea level change (excl. Antarctica)). As shown in Figure 2, elastic VLM values

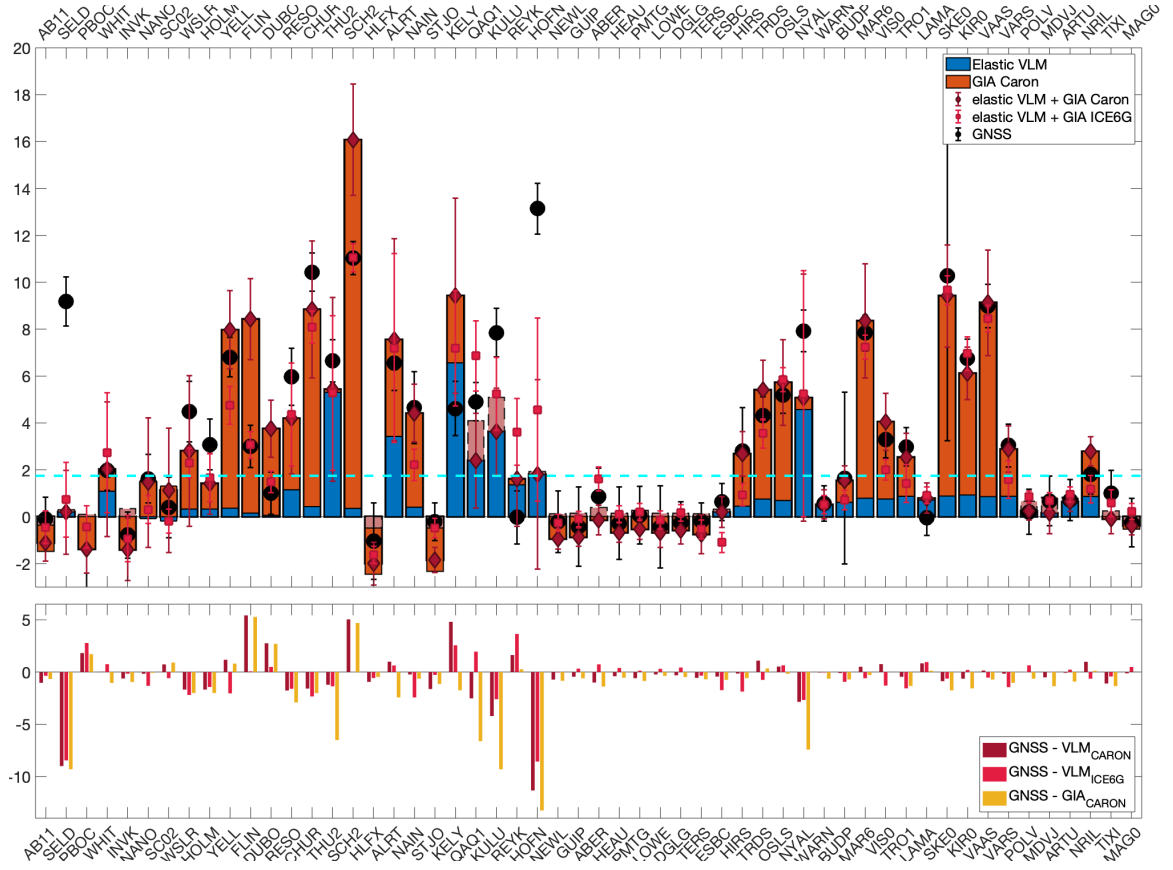


Figure 2. Average VLM change (mm y^{-1}) from 2003-2015 determined using the elastic VLM model (blue) and GIA (red) at the 54 GNSS-sites from Figure 1 and Supporting Information Figure S4.1 are shown (top). Sites are listed from most west (left) to most east (right). The dotted-cyan line indicates the average barystatic sea level rise ($\sim 1.85 \text{ mm y}^{-1}$) from the ice loss used in this study. The total modeled VLM uncertainty are indicated with red error bars and the GNSS-measured VLM is shown with black errorbars. Light red indicates locations in which GIA is negative and overlaps the positive elastic VLM. Residuals between GNSS-measured VLM ($\text{VLM}_{\text{GNSS}}^{\text{CM}}$) and the VLM-model ($\text{VLM}_{\text{model}}^{\text{CM}}$) (blue) and GIA (red) are shown (bottom). The average of the absolute residuals (equivalent to mean absolute error) are 1.45 mm y^{-1} and 1.98 mm y^{-1} respectively. All values used in this figure are included within Table S4.1 in Supporting Information.

between $0.5\text{-}1 \text{ mm y}^{-1}$ were observed at many far field GNSS-sites in this study and partly mitigated the barystatic sea level change.

The effect of non-cryospheric mass change is not included in $\text{VLM}_{\text{model}}^{\text{CM}}$. In particular terrestrial water storage (TWS) causes a small uplift over large parts of North America ($0.4 - 0.8 \text{ mm y}^{-1}$) and North-Central Siberia ($0.2 - 0.4 \text{ mm y}^{-1}$), while TWS is causing a subsidence in most of Scandinavia of $0.2 - 0.4 \text{ mm y}^{-1}$ (Frederikse et al., 2019).

Glaciated regions show particularly large residuals between the predicted VLM and VLM measured by GNSS (Figure 3), but also exhibit the largest associated uncertainties of GNSS estimates. Predicted VLM at 26 of 54 GNSS-sites are within a range of 0.75 mm y^{-1} to GNSS (the three center bins in the right panel of Figure 3). The VLM-model has a tendency to underestimate the GNSS-measured VLM, which is evident in North

America and Europe. From figure 2, we see that a different choice of GIA-model would yield enhance the accuracy of the VLM-model in these regions. The most significant discrepancies between measured and predicted VLM is explained in the following for every region.

3.1 North America

Alaska is located in the transition zone between GIA-uplift and GIA-subsidence, which is also reflected in the GNSS-rates. Nome (AB11), Prudhoe Bay (PBOC) and Inuvik (INVK) all experience an GIA-subsidence that is larger than the elastic uplift. While Nome and INVK are well matched with VLM_{GNSS}^{CM} , PBOC has the largest measured subsidence ($3.2 \pm 1.6 \text{ mm yr}^{-1}$), while VLM_{model}^{CM} only shows a subsidence of $1.4 \pm 1.4 \text{ mm yr}^{-1}$. An extraordinary subsidence is likely caused by oil extraction in the Prudhoe Bay area.

The Alaska south coast accounts for more than 25% of the total glacial melt and is naturally dominated by elastic uplift while the uplift from GIA is below 1 mm yr^{-1} . Seldovia (SELD) shows an observed average rate of $9.2 \pm 1.0 \text{ mm yr}^{-1}$, while VLM_{ela}^{CM} is only $0.3 \pm 1.6 \text{ mm yr}^{-1}$ and GIA-rate $-0.1 \pm 0.8 \text{ mm yr}^{-1}$. Seldovia is located on the Kenai Peninsula close to the Kenai Fjords, which experienced an accelerated glacial ice loss in the 20th century (VanLooy et al., 2006). This is, however, not enough to explain the increased measured uplift. GIA-estimates vary in the region (Larsen et al., 2005; Hu & Freymueller, 2019), but is not more than around $1\text{-}2 \text{ mm yr}^{-1}$. The residual seems explained by a postseismic signal following the Prince William Sound Earthquake in 1964 (Cohen & Freymueller, 2001; Huang et al., 2020) which is still causing a local uplift on this side of the peninsula. The residuals estimates this effect to be 9.0 mm yr^{-1} from 2003-2015, which is slightly less than the value found by Cohen and Freymueller (2001) of 9.3 mm yr^{-1} from 1994-2001. This rebound is expected to decay further over time, but will still be relevant for decades to come (Cohen & Freymueller, 2001; Huang et al., 2020).

Discrepancies between GNSS and modeled VLM in central North America, are likely due to uncertain GIA-estimates. A significantly better alignment between VLM_{model}^{CM} and GNSS is reached if Caron2018 is replaced by ICE-6G. The GIA-overestimate of Caron2018 in North America has been demonstrated by other studies (Schumacher et al., 2018; Frederikse et al., 2019) and is likely caused by large differences between estimated viscosity properties of paleo-RSL indicators and GNSS in North America (Caron et al., 2018). TWS-change causes a small uplift below 1 mm yr^{-1} over large parts of North America (Frederikse et al., 2019), which enhances the difference between VLM_{model}^{CM} and VLM_{GNSS}^{CM} .

3.2 Greenland

Four GNSS-sites on Greenland and Alert (ALRT) on Baffin Island measure a significant elastic uplift. While Pittuffik/Thule (THU2) and ALRT agree with VLM_{model}^{CM} , Kangerlussuaq (KELY) is overestimated quite a bit and VLM_{model}^{CM} at Kulusuk (KULU) and Qaqortoq (QAQ1) is below VLM_{GNSS}^{CM} . GIA on Greenland is poorly constrained in Caron2018, which can exaggerate VLM-estimates from GIA. A low-viscosity zone stretching from Iceland beneath Southeast Greenland (S. A. Khan et al., 2016) enables a significant viscoelastic rebound caused by ice loss since LIA (S. Khan et al., 2014).

3.3 Iceland

The two GNSS-sites on Iceland show very different uplift rates of $0.0 \pm 1.1 \text{ mm yr}^{-1}$ in Reykjavik (REYK) and $13.1 \pm 1.1 \text{ mm yr}^{-1}$ at Hoefn (HOFN) at the southern edge of the largest ice cap on Iceland, Vatnajökull. VLM_{model}^{CM} overestimates the rebound in Reykjavik while it largely underestimates it at Hoefn. Similar to south east Greenland a soft viscoelastic mantle layer (Fleming et al., 2007) creates a present-day viscoelas-

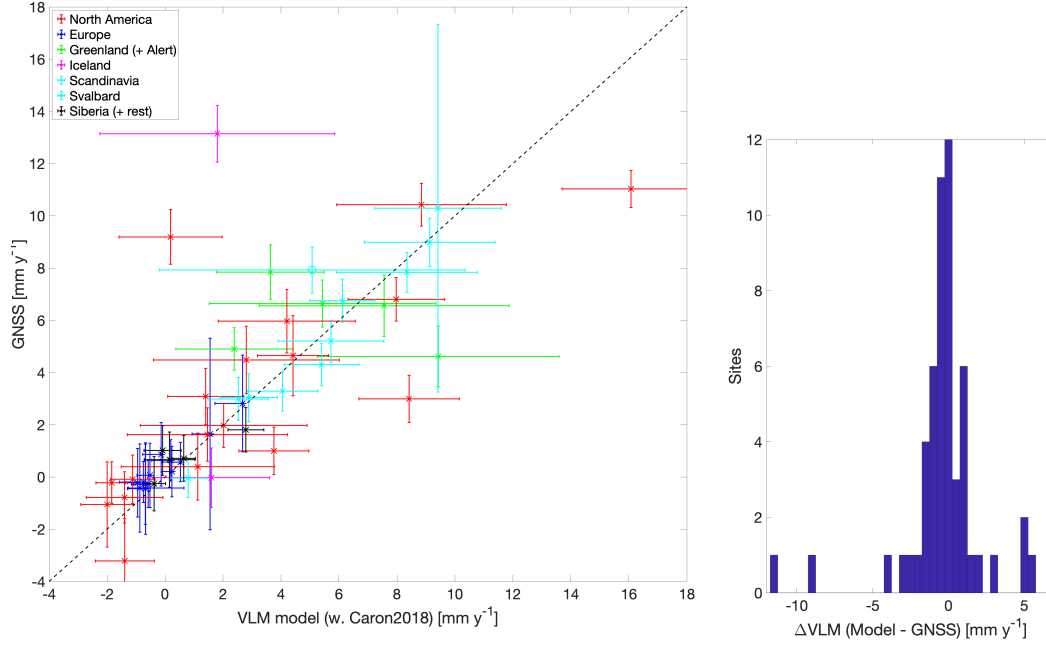


Figure 3. VLM_{GNSS}^{CM} versus VLM_{model}^{CM} including associated uncertainties for all GNSS-sites. If the cross is above the dashed line the VLM_{model}^{CM} underestimate compared to VLM_{GNSS}^{CM} . A histogram of the difference between VLM_{model}^{CM} and VLM_{GNSS}^{CM} (in intervals of 0.5 mm y^{-1}) is shown in the right panel.

tic signal that is much larger than the ones predicted by the GIA-model. A thin crust, also means that the uplift decreases faster with distance to the glacier (Fleming et al., 2007; Sørensen et al., 2017), which could explain why Reykjavik shows little vertical deformation despite being less than 100 km from glaciers.

3.4 Svalbard

The majority of land in Svalbard is covered with ice, and VLM is highly affected by ongoing ice-mass changes. At Ny Ålesund (NYAL), located on the west coast, VLM_{model}^{CM} is dominated by VLM_{ela}^{CM} of $4.6 \pm 5.3 \text{ mm yr}^{-1}$ and VLM_{GIA} of $0.5 \pm 0.4 \text{ mm yr}^{-1}$. In total this is 2.6 mm yr^{-1} short of observed VLM_{GNSS}^{CM} . While ICE6G and Caron2018 agree within $\pm 0.2 \text{ mm yr}^{-1}$, more focused, but older studies predict a slightly higher GIA contribution of around 1.5 mm yr^{-1} (Sato et al., 2006; Kierulf et al., 2009). Also on Svalbard, significant post-LIA deglaciation (Grove, 2001) is likely contributing to an ongoing uplift (Mémin et al., 2014; Rajner, 2018). The effect is still uncertain (Rajner, 2018) and Mémin et al. (2014) estimated the post-LIA rebound to be $2\text{--}5 \text{ mm yr}^{-1}$ in the beginning of 21st century, which explains the residual of 2.9 mm yr^{-1} .

3.5 Northern Europe and Scandinavia

GIA is dominating the vertical deformation in Scandinavia (Figure 1). Even though small glaciers exist in Norway, the elastic effect is very local and has almost negligible effect on the GNSS-sites in this study. However, VLM_{ela}^{CM} is still significant, and improves the correlation with observed VLM_{GNSS}^{CM} compared to a GIA-only model. This becomes more prominent for GNSS-sites in areas, where GIA is less dominant. Esbjerg (ESBC) on the west coast of Denmark is close to the zero-line of Caron2018 (-0.1 mm yr^{-1}), but

is still measuring an uplift of about 0.6 mm yr^{-1} , which is partly explained by an elastic uplift of 0.3 mm yr^{-1} .

In Northern Europe, Caron2018 models a subsidence, which is mitigated by an elastic uplift caused by present day ice melt. Generally, VLM_{model}^{CM} is consistent with VLM_{GNSS}^{CM} in the North Sea and the Baltic region, while an VLM-model using ICE6G is at odds at several locations.

3.6 Siberia

Only a few available GNSS measurements exist in eastern Europe and Siberia. Caron2018 is also challenged by limited resources of paleo sea-level records, which makes the GIA-model more dependent on the existing GNSS-records. It is commonly anticipated that Siberia had little or no ice during the last glacial cycle (Whitehouse et al., 2007), except north central Siberia and in the shallow waters in the Barents Sea between Svalbard and Novaya Zemlya (Root et al., 2015).

Also VLM_{ela}^{CM} is generally smaller than around 1 mm yr^{-1} . While the VLM_{GNSS}^{CM} is within the uncertainty-range of VLM_{model}^{CM} for the Siberian GNSS-sites (Arti (ARTU), Norilsk (NRIL), Tixi (TIXI) and Magadan (MAG0)), a GIA-only model has a better fit to the GNSS measurements which is likely due to increased dependence on GNSS in Caron2018.

4 Discussion and Conclusion

VLM of the wider Arctic region occurs mainly as a result GIA and elastic VLM. Though this study is limited to the area surrounding the Arctic, VLM caused by deglaciation produces global effects (Riva et al., 2017; Kleinherenbrink et al., 2018; Frederikse et al., 2019). By combining deglaciation that occurred since the last glacial maximum (GIA) and present-day changes in land ice (elastic VLM), the VLM-model provides a realistic estimate of VLM in the Arctic. By evaluating 54 GNSS-sites using a combined VLM-model, we found that measured uplift of GNSS can be explained by either prehistoric or present-day changes in land ice volume. For 46 of the GNSS sites, residuals between GNSS-measured VLM values and the VLM-model were smaller than associated uncertainties.

The 2x2-km spatial resolution of the used ice-model was much higher than similar gravimetric satellite observations from GRACE (Adhikari et al., 2019). Increased spatial resolution improves VLM predictions accuracy in glaciated regions significantly, as local elastic deformation tends to dominate regional averages observed via GRACE (Frederikse et al., 2019). A VLM-model to GNSS comparison also indicated that the VLM-model was inadequate in some regions due to local causes of VLM that were not included in the VLM-model, such as subsurface properties, past seismic activity or 19–20th century ice-loss (Mémin et al., 2014; Rajner, 2018).

In non-glaciated areas, GNSS measurements generally agree well with the VLM-model. Contour lines shown in Figure 1, indicate that elastic uplift is centered around Greenland, except when close to other glaciated regions (e.g. Alaska and Svalbard), despite the fact that total Arctic glaciers mass loss is comparable with that of Greenland. Hence, the elastic uplift caused by ice melt in Greenland significantly affects the entire wider Arctic region, which includes coastlines of Northern Europe and the North American Atlantic.

Riva et al. (2017) showed that elastic uplift caused by ice loss in Greenland causes a subsidence in the Southern Hemisphere. Similar, it is assumed that Antarctic ice loss will cause a subsidence in the Northern Hemisphere. Antarctic ice loss averaged 105 Gt yr^{-1} from 2003-2015 (Schröder et al., 2019), and resulted in an elastic subsidence of less than 0.1 mm yr^{-1} in the Northern Hemisphere. Since ice loss has the potential to occur

rapidly in the future (Hay et al., 2017; Edwards et al., 2019), VLM caused by Antarctic ice loss will be increasingly significant, and may be important for future coastal sea level projections in the Northern Hemisphere.

Acknowledgments

We wish to thank Lambert Caron, Matt King and one anonymous reviewer for their constructive and helpful comments, which greatly improved the manuscript. Thanks to Danielle Melini (Melini et al., 2014), for creating the REAR-code, which facilitated the creation of the VLM-model. We also greatly appreciate the work of L. Caron (Caron et al., 2018) on the Caron2018 GIA-model available from the NASA JPL website (<https://ves1.jpl.nasa.gov/solid-earth/gia/>) and R. Peltier on the ICE-6G_D model (Peltier et al., 2018). elastic VLM and both GIA-models is available in a Arctic 5x5 km grid at data.dtu.dk/articles/Arctic_Vertical_Land_Motion_5x5_km_/12554489. The project was partially funded by the EU-INTAROS project (Grant agreement no. 727890) and the ESA-Climate Change Initiative Sea level budget closure (Expro RFP/3-14679/16/I-NB).

References

- Abram, N., Adler, C., Bindoff, N., Cheng, L., Cheong, S.-M., Cheung, W., ... Zhai, P. (2019, 09). Summary for policymakers. in: IPCC special report on the ocean and cryosphere in a changing climate..
- Adhikari, S., Ivins, E. R., Frederikse, T., Landerer, F. W., & Caron, L. (2019). Sea-level fingerprints emergent from grace mission data. *Earth System Science Data*, 11(2), 629–646. Retrieved from <https://www.earth-syst-sci-data.net/11/629/2019/> doi: 10.5194/essd-11-629-2019
- Adhikari, S., Ivins, E. R., & Larour, E. (2016). Issm-sesaw v1.0: mesh-based computation of gravitationally consistent sea-level and geodetic signatures caused by cryosphere and climate driven mass change. *Geoscientific Model Development*, 9(3), 1087–1109. Retrieved from <https://www.geosci-model-dev.net/9/1087/2016/> doi: 10.5194/gmd-9-1087-2016
- Altamimi, Z., Collilieux, X., & Métivier, L. (2011). Itrf2008: an improved solution of the international terrestrial reference frame. *Journal of Geodesy*, 85(8), 457–473. Retrieved from <https://doi.org/10.1007/s00190-011-0444-4> doi: 10.1007/s00190-011-0444-4
- Argus, D., Peltier, W., Drummond, R., & Moore, A. (2014). The antarctica component of postglacial rebound model ice-6g_c (vm5a) based on gps positioning, exposure age dating of ice thicknesses, and relative sea level histories. *Geophysical Journal International*, 198(1), 537–563. Retrieved from <https://www.scopus.com/inward/record.uri?eid=2-s2.0-84905924704&doi=10.1093%2fgji%2fggu140&partnerID=40&md5=10f1208c9a63c67153b06b8bd607a133> (cited By 149) doi: 10.1093/gji/ggu140
- Bizouard, C., & Gambis, D. (2009, 06). The combined solution c04 for earth orientation parameters consistent with international terrestrial reference frame 2005. In (Vol. 134, p. 265–270). doi: 10.1007/978-3-642-00860-3_41
- Caron, L., Ivins, E. R., Larour, E., Adhikari, S., Nilsson, J., & Blewitt, G. (2018). Gia model statistics for grace hydrology, cryosphere, and ocean science. *Geophysical Research Letters*, 45(5), 2203–2212. Retrieved from <https://agupubs.onlinelibrary.wiley.com/doi/abs/10.1002/2017GL076644> doi: 10.1002/2017GL076644
- Church, J., & White, N. (2011). Sea-level rise from the late 19th to the early 21st century. *Surveys in Geophysics*, 32(4–5), 585–602. Retrieved from <https://www.scopus.com/inward/record.uri?eid=2-s2.0-80053195533&doi=10.1007%2fs10712-011-9119-1&partnerID=40&md5=>

- a6a2b9bb53f622e9bf4b3266a27d54f0 (cited By 737) doi: 10.1007/s10712-011-9119-1
- Ciraci, E., Velicogna, I., & Sutterley, T. C. (2018). Mass balance of novaya zemlya archipelago, russian high arctic, using time-variable gravity from grace and altimetry data from icesat and cryosat-2. *Remote Sensing*, 10(11). Retrieved from <https://www.mdpi.com/2072-4292/10/11/1817> doi: 10.3390/rs10111817
- Clark, J. A., & Lingle, C. S. (1977). Future sea-level changes due to west antarctic ice sheet fluctuations. *Nature*, 269(5625), 206–209. Retrieved from <https://doi.org/10.1038/269206a0> doi: 10.1038/269206a0
- Cohen, S. C., & Freymueller, J. T. (2001). Crustal uplift in the south central alaska subduction zone: New analysis and interpretation of tide gauge observations. *Journal of Geophysical Research: Solid Earth*, 106(B6), 11259–11270. Retrieved from <https://agupubs.onlinelibrary.wiley.com/doi/abs/10.1029/2000JB900419> doi: 10.1029/2000JB900419
- Dong, D., Yunck, T., & Heflin, M. (2003). Origin of the international terrestrial reference frame. *Journal of Geophysical Research: Solid Earth*, 108(B4). Retrieved from <https://agupubs.onlinelibrary.wiley.com/doi/abs/10.1029/2002JB002035> doi: 10.1029/2002JB002035
- Dziewonski, A. M., & Anderson, D. L. (1981). Preliminary reference earth model. *Physics of the Earth and Planetary Interiors*, 25(4), 297 - 356. Retrieved from <http://www.sciencedirect.com/science/article/pii/0031920181900467> doi: [https://doi.org/10.1016/0031-9201\(81\)90046-7](https://doi.org/10.1016/0031-9201(81)90046-7)
- Edwards, T., Brandon, M., Durand, G., Edwards, N., Golledge, N., Holden, P., ... Wernecke, A. (2019, 02). Revisiting antarctic ice loss due to marine ice-cliff instability. *Nature*, 566, 58–64. doi: 10.1038/s41586-019-0901-4
- Ewert, H., Groh, A., & Dietrich, R. (2012, September). Volume and mass changes of the Greenland ice sheet inferred from ICESat and GRACE. *Journal of Geodynamics*, 59–60, 111–123. doi: 10.1016/j.jog.2011.06.003
- Farrell, W. E. (1972). Deformation of the earth by surface loads. *Reviews of Geophysics*, 10(3), 761–797. Retrieved from <https://agupubs.onlinelibrary.wiley.com/doi/abs/10.1029/RG010i003p00761> doi: 10.1029/RG010i003p00761
- Farrell, W. E., & Clark, J. A. (1976). On postglacial sea level. *Geophysical Journal of the Royal Astronomical Society*, 46(3), 647–667. Retrieved from <https://onlinelibrary.wiley.com/doi/abs/10.1111/j.1365-246X.1976.tb01252.x> doi: 10.1111/j.1365-246X.1976.tb01252.x
- Fleming, K., Martinec, Z., & Wolf, D. (2007, 01). Glacial-isostatic adjustment and the viscosity structure underlying the vatnajökull ice cap, iceland. *Pure and Applied Geophysics*, 164, 751–768. doi: 10.1007/s00024-007-0187-6
- Foresta, L., Gourmelen, N., Pálsson, F., Nienow, P., Björnsson, H., & Shepherd, A. (2016). Surface elevation change and mass balance of icelandic ice caps derived from swath mode cryosat-2 altimetry. *Geophysical Research Letters*, 43(23), 12,138–12,145. Retrieved from <https://agupubs.onlinelibrary.wiley.com/doi/abs/10.1002/2016GL071485> doi: 10.1002/2016GL071485
- Forget, G., Campin, J.-M., Heimbach, P., Hill, C. N., Ponte, R. M., & Wunsch, C. (2015). Ecco version 4: an integrated framework for non-linear inverse modeling and global ocean state estimation. *Geoscientific Model Development*, 8(10), 3071–3104. Retrieved from <https://gmd.copernicus.org/articles/8/3071/2015/> doi: 10.5194/gmd-8-3071-2015
- Frederikse, T., Landerer, F. W., & Caron, L. (2019). The imprints of contemporary mass redistribution on local sea level and vertical land motion observations. *Solid Earth*, 10(6), 1971–1987. Retrieved from <https://www.solid-earth.net/10/1971/2019/> doi: 10.5194/se-10-1971-2019
- Fukumori, I., Wang, O., Fenty, I., Forget, G., Heimbach, P., & Ponte, R. M. (2019).

- Ecco version 4 release 4 dataset. <https://ecco.jpl.nasa.gov/drive>. (Accessed: 2020-06-25)
- Grove, J. (2001, 01). The initiation of the "little ice age" in regions round the north atlantic. *Climatic Change*, 48, 53-82. doi: 10.1023/A:1005662822136
- Hay, C. C., Lau, H. C. P., Gomez, N., Austermann, J., Powell, E., Mitrovica, J. X., ... Wiens, D. A. (2017). Sea level fingerprints in a region of complex earth structure: The case of wais. *Journal of Climate*, 30(6), 1881-1892. Retrieved from <https://doi.org/10.1175/JCLI-D-16-0388.1> doi: 10.1175/JCLI-D-16-0388.1
- Helm, V., Humbert, A., & Miller, H. (2014). Elevation and elevation change of greenland and antarctica derived from cryosat-2. *The Cryosphere*, 8(4), 1539-1559. Retrieved from <https://www.the-cryosphere.net/8/1539/2014/> doi: 10.5194/tc-8-1539-2014
- Henry, O., Prandi, P., Llovel, W., Cazenave, A., Jevrejeva, S., Stammer, D., ... Koldunov, N. (2012). Tide gauge-based sea level variations since 1950 along the norwegian and russian coasts of the arctic ocean: Contribution of the steric and mass components. *Journal of Geophysical Research: Oceans*, 117(C6). Retrieved from <https://agupubs.onlinelibrary.wiley.com/doi/abs/10.1029/2011JC007706> doi: 10.1029/2011JC007706
- Hu, Y., & Freymueller, J. T. (2019). Geodetic observations of time-variable glacial isostatic adjustment in southeast alaska and its implications for earth rheology. *Journal of Geophysical Research: Solid Earth*, 124(9), 9870-9889. Retrieved from <https://agupubs.onlinelibrary.wiley.com/doi/abs/10.1029/2018JB017028> doi: 10.1029/2018JB017028
- Huang, K., Hu, Y., & Freymueller, J. T. (2020). Decadal viscoelastic postseismic deformation of the 1964 mw9.2 alaska earthquake. *Journal of Geophysical Research: Solid Earth*, e2020JB019649. Retrieved from <https://agupubs.onlinelibrary.wiley.com/doi/abs/10.1029/2020JB019649> (e2020JB019649 2020JB019649) doi: 10.1029/2020JB019649
- Jevrejeva, S., Moore, J., Grinsted, A., Matthews, A., & Spada, G. (2014). Trends and acceleration in global and regional sea levels since 1807. *Global and Planetary Change*, 113, 11-22. Retrieved from <https://www.scopus.com/inward/record.uri?eid=2-s2.0-84890953576&doi=10.1016%2fj.gloplacha.2013.12.004&partnerID=40&md5=67194675f8fc061f1bb025a9fb67361f> (cited By 85) doi: 10.1016/j.gloplacha.2013.12.004
- Khan, S., Kjeldsen, K., Kjær, K., Bevan, S., Luckman, A., Aschwanden, A., ... Fitzner, A. (2014). Glacier dynamics at helheim and kangerdlugssuaq glaciers, southeast greenland, since the little ice age. *Cryosphere*, 8, 1497-1507. (CC Attribution 3.0 License) doi: 10.5194/tc-8-1497-2014
- Khan, S. A., Kjær, K. H., Korsgaard, N. J., Wahr, J., Joughin, I. R., Timm, L. H., ... Babonis, G. (2013). Recurring dynamically induced thinning during 1985 to 2010 on upernavik isstrøm, west greenland. *Journal of Geophysical Research: Earth Surface*, 118(1), 111-121. Retrieved from <https://agupubs.onlinelibrary.wiley.com/doi/abs/10.1029/2012JF002481> doi: 10.1029/2012JF002481
- Khan, S. A., Sasgen, I., Bevis, M., van Dam, T., Bamber, J. L., Wahr, J., ... Munneke, P. K. (2016). Geodetic measurements reveal similarities between post-last glacial maximum and present-day mass loss from the greenland ice sheet. *Science Advances*, 2(9). Retrieved from <https://advances.sciencemag.org/content/2/9/e1600931> doi: 10.1126/sciadv.1600931
- Kierulf, H. P., Plag, H.-P., & Kohler, J. (2009, 10). Surface deformation induced by present-day ice melting in svalbard. *Geophysical Journal International*, 179(1), 1-13. Retrieved from <https://doi.org/10.1111/j.1365-246X.2009.04322.x> doi: 10.1111/j.1365-246X.2009.04322.x
- King, M. A., Keshin, M., Whitehouse, P. L., Thomas, I. D., Milne, G., & Riva,

- 518 R. E. M. (2012). Regional biases in absolute sea-level estimates from tide
519 gauge data due to residual unmodeled vertical land movement. *Geophysical*
520 *Research Letters*, 39(14). Retrieved from [https://agupubs.onlinelibrary](https://agupubs.onlinelibrary.wiley.com/doi/abs/10.1029/2012GL052348)
521 [.wiley.com/doi/abs/10.1029/2012GL052348](https://agupubs.onlinelibrary.wiley.com/doi/abs/10.1029/2012GL052348) doi: 10.1029/2012GL052348
- 522 King, M. A., & Watson, C. S. (2014, 09). Geodetic vertical velocities affected by re-
523 cent rapid changes in polar motion. *Geophysical Journal International*, 199(2),
524 1161-1165. Retrieved from <https://doi.org/10.1093/gji/ggu325> doi: 10
525 .1093/gji/ggu325
- 526 Kjeldsen, K. K., Khan, S. A., Wahr, J., Korsgaard, N. J., Kjær, K. H., Bjørk, A. A.,
527 ... van Angelen, J. H. (2013). Improved ice loss estimate of the northwestern
528 greenland ice sheet. *Journal of Geophysical Research: Solid Earth*, 118(2),
529 698-708. Retrieved from [https://agupubs.onlinelibrary.wiley.com/doi/](https://agupubs.onlinelibrary.wiley.com/doi/abs/10.1029/2012JB009684)
530 [abs/10.1029/2012JB009684](https://agupubs.onlinelibrary.wiley.com/doi/abs/10.1029/2012JB009684) doi: 10.1029/2012JB009684
- 531 Kleinherenbrink, M., Riva, R., & Frederikse, T. (2018). A comparison of methods
532 to estimate vertical land motion trends from gnss and altimetry at tide gauge
533 stations. *Ocean Science*, 14(2), 187-204. Retrieved from [https://www.scopus](https://www.scopus.com/inward/record.uri?eid=2-s2.0-85044121271&doi=10.5194/2fos-14-187-2018&partnerID=40&md5=dbe85241ab9f3400fe3f655c42918079)
534 [.com/inward/record.uri?eid=2-s2.0-85044121271&doi=10.5194/2fos-14](https://www.scopus.com/inward/record.uri?eid=2-s2.0-85044121271&doi=10.5194/2fos-14-187-2018&partnerID=40&md5=dbe85241ab9f3400fe3f655c42918079)
535 [-187-2018&partnerID=40&md5=dbe85241ab9f3400fe3f655c42918079](https://www.scopus.com/inward/record.uri?eid=2-s2.0-85044121271&doi=10.5194/2fos-14-187-2018&partnerID=40&md5=dbe85241ab9f3400fe3f655c42918079) (cited
536 By 6) doi: 10.5194/os-14-187-2018
- 537 Krabill, W. B. (2011). *Icebridge atm l2 icesn elevation, slope, and roughness,*
538 *[1993-2012]*. (Boulder, Colorado: NASA Distributed Active Archive Center
539 at the National Snow and Ice Data Center) doi: 10.5067/ICESAT/GLAS/
540 DATA225
- 541 Kustowski, B., Dziewoński, A. M., & Ekström, G. (2007, 10). Nonlinear Crustal
542 Corrections for Normal-Mode Seismograms. *Bulletin of the Seismological Soci-*
543 *ety of America*, 97(5), 1756-1762. Retrieved from [https://doi.org/10.1785/](https://doi.org/10.1785/0120070041)
544 [0120070041](https://doi.org/10.1785/0120070041) doi: 10.1785/0120070041
- 545 Larsen, C. F., Motyka, R. J., Freymueller, J. T., Echelmeyer, K. A., & Ivins, E. R.
546 (2005). Rapid viscoelastic uplift in southeast alaska caused by post-little ice
547 age glacial retreat. *Earth and Planetary Science Letters*, 237(3), 548 - 560.
548 Retrieved from [http://www.sciencedirect.com/science/article/pii/](http://www.sciencedirect.com/science/article/pii/S0012821X05004152)
549 [S0012821X05004152](http://www.sciencedirect.com/science/article/pii/S0012821X05004152) doi: <https://doi.org/10.1016/j.epsl.2005.06.032>
- 550 Li, T., Wu, P., Wang, H., Steffen, H., Khan, N. S., Engelhart, S. E., ... Horton, B. P.
551 (2020). Uncertainties of glacial isostatic adjustment model predictions in north
552 america associated with 3d structure. *Geophysical Research Letters*, 47(10),
553 e2020GL087944. Retrieved from [https://agupubs.onlinelibrary.wiley](https://agupubs.onlinelibrary.wiley.com/doi/abs/10.1029/2020GL087944)
554 [.com/doi/abs/10.1029/2020GL087944](https://agupubs.onlinelibrary.wiley.com/doi/abs/10.1029/2020GL087944) (e2020GL087944 2020GL087944) doi:
555 10.1029/2020GL087944
- 556 Marzeion, B., Jarosch, A. H., & Hofer, M. (2012). Past and future sea-level change
557 from the surface mass balance of glaciers. *The Cryosphere*, 6(6), 1295-1322.
558 Retrieved from <https://www.the-cryosphere.net/6/1295/2012/> doi:
559 10.5194/tc-6-1295-2012
- 560 Melini, D., Gegout, P., King, M., Marzeion, B., & Spada, G. (2015, 08). On the
561 rebound: Modeling earth's ever-changing shape. *Eos Transactions American*
562 *Geophysical Union*, 96. doi: 10.1029/2015EO033387
- 563 Melini, D., Spada, G., Gegout, P., & King, M. (2014, 01). *Rear - a regional elastic*
564 *rebound calculator. user manual for version 1.0.* Retrieved from [http://hpc](http://hpc.rm.ingv.it/rear)
565 [.rm.ingv.it/rear](http://hpc.rm.ingv.it/rear)
- 566 Milne, G. A., & Mitrovica, J. X. (1998, 04). Postglacial sea-level change on a ro-
567 tating Earth. *Geophysical Journal International*, 133(1), 1-19. Retrieved
568 from <https://doi.org/10.1046/j.1365-246X.1998.1331455.x> doi:
569 10.1046/j.1365-246X.1998.1331455.x
- 570 Milne, G. A., Mitrovica, J. X., & Davis, J. L. (1999, 11). Near-field hydro-isostasy:
571 the implementation of a revised sea-level equation. *Geophysical Journal Inter-*
572 *national*, 139(2), 464-482. Retrieved from <https://doi.org/10.1046/j.1365>

- 246x.1999.00971.x doi: 10.1046/j.1365-246x.1999.00971.x
- Mémin, A., Spada, G., Boy, J.-P., Rogister, Y., & Hinderer, J. (2014, 05). Decadal geodetic variations in Ny-Ålesund (Svalbard): role of past and present ice-mass changes. *Geophysical Journal International*, 198(1), 285-297. Retrieved from <https://doi.org/10.1093/gji/ggu134> doi: 10.1093/gji/ggu134
- Nerem, R. S., Beckley, B. D., Fasullo, J. T., Hamlington, B. D., Masters, D., & Mitchum, G. T. (2018). Climate-change-driven accelerated sea-level rise detected in the altimeter era. *Proceedings of the National Academy of Sciences*, 115(9), 2022–2025. Retrieved from <https://www.pnas.org/content/115/9/2022> doi: 10.1073/pnas.1717312115
- Nuth, C., Moholdt, G., Kohler, J., Hagen, J. O., & Kääb, A. (2010). Svalbard glacier elevation changes and contribution to sea level rise. *Journal of Geophysical Research: Earth Surface*, 115(F1). Retrieved from <https://agupubs.onlinelibrary.wiley.com/doi/abs/10.1029/2008JF001223> doi: 10.1029/2008JF001223
- Peltier, W., Argus, D., & Drummond, R. (2015). Space geodesy constrains ice age terminal deglaciation: The global ice-6g-c (vm5a) model. *Journal of Geophysical Research: Solid Earth*, 120(1), 450-487. Retrieved from <https://www.scopus.com/inward/record.uri?eid=2-s2.0-85027948080&doi=10.1002/2f2014JB011176&partnerID=40&md5=29a7ce38c5cf3872d2276981d2f6b34f> (cited By 326) doi: 10.1002/2014JB011176
- Peltier, W. R., Argus, D. F., & Drummond, R. (2018, February). Comment on "An Assessment of the ICE-6G_C (VM5a) Glacial Isostatic Adjustment Model" by Purcell et al. *Journal of Geophysical Research (Solid Earth)*, 123(2), 2019–2028. doi: 10.1002/2016JB013844
- Pfeffer, W. T., Arendt, A. A., Bliss, A., Bolch, T., Cogley, J. G., Gardner, A. S., ... et al. (2014). The randolph glacier inventory: a globally complete inventory of glaciers. *Journal of Glaciology*, 60(221), 537–552. doi: 10.3189/2014JoG13J176
- Post, E., Alley, R. B., Christensen, T. R., Macias-Fauria, M., Forbes, B. C., Gooseff, M. N., ... Wang, M. (2019). The polar regions in a 2c warmer world. *Science Advances*, 5(12). Retrieved from <https://advances.sciencemag.org/content/5/12/eaaw9883> doi: 10.1126/sciadv.aaw9883
- Rajner, M. (2018). Detection of ice mass variation using gnss measurements at svalbard. *Journal of Geodynamics*, 121, 20 - 25. Retrieved from <http://www.sciencedirect.com/science/article/pii/S0264370718300450> doi: <https://doi.org/10.1016/j.jog.2018.06.001>
- RGI Consortium. (2017). *Randolph Glacier Inventory – A Dataset of Global Glacier Outlines: Version 6.0: Technical Report*. (<https://doi.org/10.7265/N5-RGI-60>)
- Riva, E., Frederikse, T., King, A., Marzeion, B., & Van Den Broeke, R. (2017). Brief communication: The global signature of post-1900 land ice wastage on vertical land motion. *Cryosphere*, 11(3), 1327-1332. Retrieved from <https://www.scopus.com/inward/record.uri?eid=2-s2.0-85020484420&doi=10.5194/2ftc-11-1327-2017&partnerID=40&md5=077251aec38900cef0ec0ecdd2b1eded> (cited By 11) doi: 10.5194/2ftc-11-1327-2017
- Root, B. C., Tarasov, L., & van der Wal, W. (2015). Grace gravity observations constrain weichselian ice thickness in the barents sea. *Geophysical Research Letters*, 42(9), 3313-3320. Retrieved from <https://agupubs.onlinelibrary.wiley.com/doi/abs/10.1002/2015GL063769> doi: 10.1002/2015GL063769
- Santamaría-Gómez, A., Gravelle, M., Dangendorf, S., Marcos, M., Spada, G., & Wöppelmann, G. (2017). Uncertainty of the 20th century sea-level rise due to vertical land motion errors. *Earth and Planetary Science Letters*, 473, 24 - 32. Retrieved from <http://www.sciencedirect.com/science/article/pii/S0012016817321111>

- S0012821X17303060 doi: <https://doi.org/10.1016/j.epsl.2017.05.038>
- Santamaría-Gómez, A., & Mémin, A. (2015, 05). Geodetic secular velocity errors due to interannual surface loading deformation. *Geophysical Journal International*, 202(2), 763–767. Retrieved from <https://doi.org/10.1093/gji/ggv190> doi: 10.1093/gji/ggv190
- Sato, T., Okuno, J., Hinderer, J., MacMillan, D. S., Plag, H.-P., Francis, O., ... Fukuda, Y. (2006, 06). A geophysical interpretation of the secular displacement and gravity rates observed at Ny-Ålesund, Svalbard in the Arctic—effects of post-glacial rebound and present-day ice melting. *Geophysical Journal International*, 165(3), 729–743. Retrieved from <https://doi.org/10.1111/j.1365-246X.2006.02992.x> doi: 10.1111/j.1365-246X.2006.02992.x
- Schröder, L., Horwath, M., Dietrich, R., Helm, V., van den Broeke, M. R., & Ligtenberg, S. R. M. (2019). Four decades of antarctic surface elevation changes from multi-mission satellite altimetry. *The Cryosphere*, 13(2), 427–449. Retrieved from <https://www.the-cryosphere.net/13/427/2019/> doi: 10.5194/tc-13-427-2019
- Schumacher, M., King, M., Rougier, J., Sha, Z., Khan, S. A., & Bamber, J. (2018). A new global gps data set for testing and improving modelled glacial uplift rates. *Geophysical Journal International*, 214(3), 2164–2176. Retrieved from <https://www.scopus.com/inward/record.uri?eid=2-s2.0-85050475763&doi=10.1093%2fgji%2fggy235&partnerID=40&md5=0b6d3ed0cdf0208346d1d8bb4bed2c40> (cited By 5) doi: 10.1093/gji/ggy235
- Simon, K. M., Riva, R. E. M., Kleinenherbrink, M., & Frederikse, T. (2018). The glacial isostatic adjustment signal at present day in northern europe and the british isles estimated from geodetic observations and geophysical models. *Solid Earth*, 9(3), 777–795. Retrieved from <https://www.solid-earth.net/9/777/2018/> doi: 10.5194/se-9-777-2018
- Smith, B. E., Fricker, H. A., Joughin, I. R., & Tulaczyk, S. (2009). An inventory of active subglacial lakes in antarctica detected by icesat (2003–2008). *Journal of Glaciology*, 55(192), 573–595. doi: 10.3189/002214309789470879
- Sun, Y., Riva, R., & Ditmar, P. (2016). Optimizing estimates of annual variations and trends in geocenter motion and j2 from a combination of grace data and geophysical models. *Journal of Geophysical Research: Solid Earth*, 121(11), 8352–8370. Retrieved from <https://agupubs.onlinelibrary.wiley.com/doi/abs/10.1002/2016JB013073> doi: 10.1002/2016JB013073
- Sørensen, L. S., Jarosch, A. H., Adalgeirsdóttir, G., Barletta, V. R., Forsberg, R., Pálsson, F., ... Jóhannesson, T. (2017, 01). The effect of signal leakage and glacial isostatic rebound on GRACE-derived ice mass changes in Iceland. *Geophysical Journal International*, 209(1), 226–233. Retrieved from <https://doi.org/10.1093/gji/ggx008> doi: 10.1093/gji/ggx008
- Tapley, B. D., Bettadpur, S., Watkins, M., & Reigber, C. (2004). The gravity recovery and climate experiment: Mission overview and early results. *Geophysical Research Letters*, 31(9). Retrieved from <https://agupubs.onlinelibrary.wiley.com/doi/abs/10.1029/2004GL019920> doi: 10.1029/2004GL019920
- Tushingham, A. M., & Peltier, W. R. (1991). Ice-3g: A new global model of late pleistocene deglaciation based upon geophysical predictions of post-glacial relative sea level change. *Journal of Geophysical Research: Solid Earth*, 96(B3), 4497–4523. Retrieved from <https://agupubs.onlinelibrary.wiley.com/doi/abs/10.1029/90JB01583> doi: 10.1029/90JB01583
- van Dam, T., Collilieux, X., Wuite, J., Altamimi, Z., & Ray, J. (2012). Nontidal ocean loading: amplitudes and potential effects in gps height time series. *Journal of Geodesy*, 86(11), 1043–1057. Retrieved from <https://doi.org/10.1007/s00190-012-0564-5> doi: 10.1007/s00190-012-0564-5
- VanLooy, J., Forster, R., & Ford, A. (2006). Accelerating thinning of kenai peninsula glaciers, alaska. *Geophysical Research Letters*, 33(21). Retrieved

- from <https://agupubs.onlinelibrary.wiley.com/doi/abs/10.1029/2006GL028060> doi: 10.1029/2006GL028060
- Wang, H., Xiang, L., Jia, L., Jiang, L., Wang, Z., Hu, B., & Gao, P. (2012). Load love numbers and green's functions for elastic earth models prem, iasp91, ak135, and modified models with refined crustal structure from crust 2.0. *Computers & Geosciences*, 49, 190 - 199. Retrieved from <http://www.sciencedirect.com/science/article/pii/S0098300412002245> doi: <https://doi.org/10.1016/j.cageo.2012.06.022>
- Watson, C. S., White, N. J., Church, J. A., King, M. A., Burgette, R. J., & Legresy, B. (2015, JUN). Unabated global mean sea-level rise over the satellite altimeter era. *NATURE CLIMATE CHANGE*, 5(6), 565+.
- Whitehouse, P. L., Allen, M. B., & Milne, G. A. (2007, 08). Glacial isostatic adjustment as a control on coastal processes: An example from the Siberian Arctic. *Geology*, 35(8), 747-750. Retrieved from <https://doi.org/10.1130/G23437A.1> doi: 10.1130/G23437A.1
- Wöppelmann, G., & Marcos, M. (2016). Vertical land motion as a key to understanding sea level change and variability. *Reviews of Geophysics*, 54(1), 64-92. Retrieved from <https://agupubs.onlinelibrary.wiley.com/doi/abs/10.1002/2015RG000502> doi: 10.1002/2015RG000502
- Zemp, M., Huss, M., Thibert, E., Eckert, N., McNabb, R., Huber, J., ... Cogley, J. G. (2019). Global glacier mass changes and their contributions to sea-level rise from 1961 to 2016. *Nature*, 568(7752), 382-386. doi: 10.1038/s41586-019-1071-0
- Zwally, H. J., Schutz, R., Bentley, C., Bufton, J., Herring, T., Minster, J., ... Thomas, R. (2011). *Glas/icesat l2 antarctic and greenland ice sheet altimetry data v031*. (Boulder, Colorado: NASA Distributed Active Archive Center at the National Snow and Ice Data Center) doi: 10.5067/CPRXXK3F39RV

References of Supporting Information:

- Caron, L., Ivins, E. R., Larour, E., Adhikari, S., Nilsson, J., & Blewitt, G. (2018). Gia model statistics for grace hydrology, cryosphere, and ocean science. *Geophysical Research Letters*, 45(5), 2203-2212. Retrieved from <https://agupubs.onlinelibrary.wiley.com/doi/abs/10.1002/2017GL076644> doi: 10.1002/2017GL076644
- Cohen, S. C., & Freymueller, J. T. (2001). Crustal uplift in the south central alaska subduction zone: New analysis and interpretation of tide gauge observations. *Journal of Geophysical Research: Solid Earth*, 106(B6), 11259-11270. Retrieved from <https://agupubs.onlinelibrary.wiley.com/doi/abs/10.1029/2000JB900419> doi: 10.1029/2000JB900419
- Fleming, K., Martinec, Z., & Wolf, D. (2007, 01). Glacial-isostatic adjustment and the viscosity structure underlying the vatnajökull ice cap, iceland. *Pure and Applied Geophysics*, 164, 751-768. doi: 10.1007/s00024-007-0187-6
- Frederikse, T., Landerer, F. W., & Caron, L. (2019). The imprints of contemporary mass redistribution on local sea level and vertical land motion observations. *Solid Earth*, 10(6), 1971-1987. Retrieved from <https://www.solid-earth.net/10/1971/2019/> doi: 10.5194/se-10-1971-2019
- Grove, J. (2001, 01). The initiation of the "little ice age" in regions round the north atlantic. *Climatic Change*, 48, 53-82. doi: 10.1023/A:1005662822136
- Hu, Y., & Freymueller, J. T. (2019). Geodetic observations of time-variable glacial isostatic adjustment in southeast alaska and its implications for earth rheology. *Journal of Geophysical Research: Solid Earth*, 124(9), 9870-9889. Retrieved from <https://agupubs.onlinelibrary.wiley.com/doi/abs/10.1029/2018JB017028> doi: 10.1029/2018JB017028
- Kierulf, H. P., Plag, H.-P., & Kohler, J. (2009, 10). Surface deformation induced by

- present-day ice melting in Svalbard. *Geophysical Journal International*, 179(1), 1-13. Retrieved from <https://doi.org/10.1111/j.1365-246X.2009.04322.x> doi: 10.1111/j.1365-246X.2009.04322.x
- King, M. A., & Watson, C. S. (2014, 09). Geodetic vertical velocities affected by recent rapid changes in polar motion. *Geophysical Journal International*, 199(2), 1161-1165. Retrieved from <https://doi.org/10.1093/gji/ggu325> doi: 10.1093/gji/ggu325
- Larsen, C. F., Motyka, R. J., Freymueller, J. T., Echelmeyer, K. A., & Ivins, E. R. (2005). Rapid viscoelastic uplift in southeast alaska caused by post-little ice age glacial retreat. *Earth and Planetary Science Letters*, 237(3), 548 - 560. Retrieved from <http://www.sciencedirect.com/science/article/pii/S0012821X05004152> doi: <https://doi.org/10.1016/j.epsl.2005.06.032>
- Mémin, A., Spada, G., Boy, J.-P., Rogister, Y., & Hinderer, J. (2014, 05). Decadal geodetic variations in Ny-Ålesund (Svalbard): role of past and present ice-mass changes. *Geophysical Journal International*, 198(1), 285-297. Retrieved from <https://doi.org/10.1093/gji/ggu134> doi: 10.1093/gji/ggu134
- Peltier, W., Argus, D., & Drummond, R. (2015). Space geodesy constrains ice age terminal deglaciation: The global ice-6g-c (vm5a) model. *Journal of Geophysical Research: Solid Earth*, 120(1), 450-487. Retrieved from <https://www.scopus.com/inward/record.uri?eid=2-s2.0-85027948080&doi=10.1002/2f2014JB011176&partnerID=40&md5=29a7ce38c5cf3872d2276981d2f6b34f> (cited By 326) doi: 10.1002/2014JB011176
- Pfeffer, W. T., Arendt, A. A., Bliss, A., Bolch, T., Cogley, J. G., Gardner, A. S., ... et al. (2014). The randolph glacier inventory: a globally complete inventory of glaciers. *Journal of Glaciology*, 60(221), 537-552. doi: 10.3189/2014JoG13J176
- Rajner, M. (2018). Detection of ice mass variation using gnss measurements at svalbard. *Journal of Geodynamics*, 121, 20 - 25. Retrieved from <http://www.sciencedirect.com/science/article/pii/S0264370718300450> doi: <https://doi.org/10.1016/j.jog.2018.06.001>
- Root, B. C., Tarasov, L., & van der Wal, W. (2015). Grace gravity observations constrain weichselian ice thickness in the barents sea. *Geophysical Research Letters*, 42(9), 3313-3320. Retrieved from <https://agupubs.onlinelibrary.wiley.com/doi/abs/10.1002/2015GL063769> doi: 10.1002/2015GL063769
- Sato, T., Okuno, J., Hinderer, J., MacMillan, D. S., Plag, H.-P., Francis, O., ... Fukuda, Y. (2006, 06). A geophysical interpretation of the secular displacement and gravity rates observed at Ny-Ålesund, Svalbard in the Arctic—effects of post-glacial rebound and present-day ice melting. *Geophysical Journal International*, 165(3), 729-743. Retrieved from <https://doi.org/10.1111/j.1365-246X.2006.02992.x> doi: 10.1111/j.1365-246X.2006.02992.x
- Schröder, L., Horwath, M., Dietrich, R., Helm, V., van den Broeke, M. R., & Ligtenberg, S. R. M. (2019). Four decades of antarctic surface elevation changes from multi-mission satellite altimetry. *The Cryosphere*, 13(2), 427-449. Retrieved from <https://www.the-cryosphere.net/13/427/2019/> doi: 10.5194/tc-13-427-2019
- Shepherd, A., Ivins, E., Rignot, E., Smith, B., van den Broeke, M., Velicogna, I., ... Wouters, B. (2018). Mass balance of the antarctic ice sheet from 1992 to 2017. *Nature*, 558(7709), 219-222. doi: 10.1038/s41586-018-0179-y
- Sun, Y., Riva, R., & Ditmar, P. (2016). Optimizing estimates of annual variations and trends in geocenter motion and j2 from a combination of grace data and geophysical models. *Journal of Geophysical Research: Solid Earth*, 121(11), 8352-8370. Retrieved from <https://agupubs.onlinelibrary.wiley.com/doi/abs/10.1002/2016JB013073> doi: 10.1002/2016JB013073
- Swenson, S., Chambers, D., & Wahr, J. (2008). Estimating geocenter variations from a combination of grace and ocean model output. *Journal of*

- 791 *Geophysical Research: Solid Earth*, 113(B8). Retrieved from [https://](https://agupubs.onlinelibrary.wiley.com/doi/abs/10.1029/2007JB005338)
792 agupubs.onlinelibrary.wiley.com/doi/abs/10.1029/2007JB005338 doi:
793 10.1029/2007JB005338
- 794 Sørensen, L. S., Jarosch, A. H., Adalgeirsdóttir, G., Barletta, V. R., Forsberg, R.,
795 Pálsson, F., ... Jóhannesson, T. (2017, 01). The effect of signal leakage
796 and glacial isostatic rebound on GRACE-derived ice mass changes in Ice-
797 land. *Geophysical Journal International*, 209(1), 226-233. Retrieved from
798 <https://doi.org/10.1093/gji/ggx008> doi: 10.1093/gji/ggx008
- 799 Tushingham, A. M., & Peltier, W. R. (1991). Ice-3g: A new global model of late
800 pleistocene deglaciation based upon geophysical predictions of post-glacial rel-
801 ative sea level change. *Journal of Geophysical Research: Solid Earth*, 96(B3),
802 4497-4523. Retrieved from [https://agupubs.onlinelibrary.wiley.com/](https://agupubs.onlinelibrary.wiley.com/doi/abs/10.1029/90JB01583)
803 [doi/abs/10.1029/90JB01583](https://agupubs.onlinelibrary.wiley.com/doi/abs/10.1029/90JB01583) doi: 10.1029/90JB01583
- 804 VanLooy, J., Forster, R., & Ford, A. (2006). Accelerating thinning of kenai
805 peninsula glaciers, alaska. *Geophysical Research Letters*, 33(21). Retrieved
806 from [https://agupubs.onlinelibrary.wiley.com/doi/abs/10.1029/](https://agupubs.onlinelibrary.wiley.com/doi/abs/10.1029/2006GL028060)
807 [2006GL028060](https://agupubs.onlinelibrary.wiley.com/doi/abs/10.1029/2006GL028060) doi: 10.1029/2006GL028060
- 808 Whitehouse, P. L., Allen, M. B., & Milne, G. A. (2007, 08). Glacial isostatic ad-
809 justment as a control on coastal processes: An example from the Siberian
810 Arctic. *Geology*, 35(8), 747-750. Retrieved from [https://doi.org/10.1130/](https://doi.org/10.1130/G23437A.1)
811 [G23437A.1](https://doi.org/10.1130/G23437A.1) doi: 10.1130/G23437A.1